

# Permutation Meets Parallel Compressed Sensing: How to Relax Restricted Isometry Property for 2D Sparse Signals

Hao Fang, Sergiy A. Vorobyov, Hai Jiang, and Omid Taheri

## Abstract

Traditional compressed sensing considers sampling a 1D signal. For a multidimensional signal, if reshaped into a vector, the required size of the sensing matrix becomes dramatically large, which increases the storage and computational complexity significantly. To solve this problem, we propose to reshape the multidimensional signal into a 2D signal and sample the 2D signal using compressed sensing column by column with the same sensing matrix. It is referred to as *parallel compressed sensing*, and it has much lower storage and computational complexity. For a given reconstruction performance of parallel compressed sensing, if a so-called *acceptable permutation* is applied to the 2D signal, we show that the corresponding sensing matrix has a smaller required order of restricted isometry property condition, and thus, storage and computation requirements are further lowered. A zigzag-scan-based permutation, which is shown to be particularly useful for signals satisfying a layer model, is introduced and investigated. As an application of the parallel compressed sensing with the zigzag-scan-based permutation, a video compression scheme is presented. It is shown that the zigzag-scan-based permutation increases the peak signal-to-noise ratio of reconstructed images and video frames.

## Index Terms

Compressed sensing, parallel processing, permutation, multidimensional signal processing.

S. A. Vorobyov is the corresponding author. All authors are with the Department of Electrical and Computer Engineering, University of Alberta, Edmonton, AB, T6G 2V4, Canada; e-mail: {hfang2, svorobyov, hail, otaheri}@ualberta.ca. S. A. Vorobyov is currently on leave and he is with Aalto University, Finland.

This work is supported in part by the Natural Science and Engineering Research Council (NSERC) of Canada.

Some initial results on which this paper is built have been presented by the authors at Asilomar 2012, Pacific Grove, California, USA.

## I. INTRODUCTION

Compressed sensing (CS) theory states that the information contained in an  $L$ -length sparse signal  $\mathbf{x}$  can be fully preserved with only  $K \ll L$  measurements, which form a  $K$ -length vector  $\mathbf{y}$  [1], [2]. This is done by the help of a  $K \times L$  *sensing matrix*  $\mathbf{A}$ , i.e.,  $\mathbf{y} = \mathbf{A}\mathbf{x}$ , where  $\mathbf{A}$  satisfies the restricted isometry property (RIP) of a certain order. The signal  $\mathbf{x}$  can be recovered from the  $K$  measurements in  $\mathbf{y}$  by solving, for example, the following  $\ell_1$ -norm minimization problem [3]

$$\min_{\mathbf{x}} \|\mathbf{x}\|_1 \text{ s.t. } \mathbf{y} = \mathbf{A}\mathbf{x} \quad (1)$$

where  $\|\cdot\|_1$  denotes the  $\ell_1$ -norm of a vector.

In addition, if signal  $\mathbf{f}$  is not sparse itself, it can be represented as a sparse signal in some orthonormal basis  $\Psi$ , i.e.,  $\mathbf{x} = \Psi^T \mathbf{f}$  is sparse signal. Here the superscript  $T$  denotes the transpose operation. Then given the sensing matrix  $\mathbf{A}$  for  $\mathbf{x}$  and the orthonormal basis  $\Psi$ , the signal  $\mathbf{f}$  can be measured using a  $K \times L$  *measurement matrix*  $\Phi = \mathbf{A}\Psi^T$ , i.e.,  $\mathbf{y} = \Phi\mathbf{f}$ . It is equivalent to using  $\mathbf{A}$  to sense  $\mathbf{x}$  since  $\mathbf{y} = \mathbf{A}\Psi^T \mathbf{f} = \mathbf{A}\mathbf{x}$ . Therefore,  $\mathbf{x}$  and thus  $\mathbf{f}$  can be recovered from  $\mathbf{y}$  as long as  $\mathbf{A}$  satisfies the RIP of a certain order. Consequently, two basic problems in CS are (i) to find the basis  $\Psi$  in which the signal projection is sparse and (ii) to construct sensing matrix  $\mathbf{A}$  and corresponding measurement matrix  $\Phi$ .

Traditionally, CS is applied to sample 1D signals. Recently, the research interest in applying CS to sample multidimensional signals has increased significantly. 2D signals such as images and video frames are typical examples of multidimensional signals. A branch of CS theory, named *compressive imaging*, is introduced in [4], where the *single-pixel camera* is proposed. The single-pixel camera acquires a group of measurements of an image using different patterns of the digital micromirror device (DMD) array, without collecting the pixels. Mathematically, each pattern of the DMD array plays the role of a row in the measurement matrix  $\Phi$ , and the image is viewed as a vector. Consequently, the size of the DMD array is the same as the expected number of pixels in the image. The research is extended to sample color images by combining the Bayer color filter and the DMD array [5]. Furthermore, for reconstruction, the architecture proposed in [5] employs joint sparsity models to exploit the correlation among different color channels. However, as the expected number of pixels in the image increases, the number of columns and the required number of rows in the measurement matrix  $\Phi$  also increase. In other words, both the size and the required number of patterns of the DMD array increase. Therefore, the implementation cost and the complexity of the encoder increase significantly as well. For example, the storage of  $\Phi$  and computational complexity for acquiring measurements are unwieldy for any normal size images. A general framework for sampling multidimensional signals, named *Kronecker CS*, is proposed

in [6]. In Kronecker CS, a multidimensional signal is vectorized and then sampled using a measurement matrix which is the Kronecker product of several smaller-sized measurement matrices that correspond to the measurement processes for different portions of the multidimensional signal<sup>1</sup>. After finding such Kronecker product, the resulting measurement matrix clearly has a very large size. Thus, the problem related to the storage of  $\Phi$  and computational complexity for acquiring measurements arises as well in the Kronecker CS.

To address the above problem, instead of storing the Kronecker product of several measurement matrices, all portions of the multidimensional signal can be sampled sequentially using corresponding smaller-sized measurement matrices. Then the encoder needs to store only the smaller-sized measurement matrices. Using this approach, a separable sensing operator is designed for compressive imaging in [7], where an imaging operator (the measurement matrix for the whole image) can be separated into two dimensions. The separable sensing operator design significantly reduces the complexity of implementation, storage, and usage of the imaging operator. Another solution to the problem of storage and computational complexity is the block CS of [8]. The idea is to divide a 2D signal into smaller blocks and sample individual vectorized blocks, whereas all blocks need to be reconstructed as a whole. The block CS of [8] uses a block-diagonal measurement matrix for sampling the vectorized signal  $\mathbf{x}$ . As a result, the block CS can reduce the storage and computational complexity at the encoder side. Some improved reconstruction algorithms for the block CS scheme are presented in [9]. They help to further reduce the required number of rows in the measurement matrix  $\Phi$  for a given reconstruction error requirement. Based on the block CS architecture, a fast sampling operator is proposed in [10] using the block Hadamard ensemble, which can be easily implemented in the optical domain.

The use of fast algorithms for computing measurements by taking advantage of the measurement matrix's structure is another way to address the problem of storage and computational complexity at the encoder side. For example, in [11] and [12], a scrambled Fourier ensemble is used as the sensing matrix  $\mathbf{A}$  and the wavelet basis is used as the orthonormal basis  $\Psi$  in which the image projection is sparse. Thus, the sampling process can be implemented efficiently by first transforming a 2D image into the wavelet domain and then applying  $\mathbf{A}$  to the wavelet coefficients by means of the fast Fourier transform. The sparsity structure of the multidimensional signal can be employed as well to reduce the storage and computational complexity at the encoder side. It is proposed in [13] to decompose the wavelet coefficients

<sup>1</sup>For example, for a 2D signal, the smaller-sized measurement matrices can correspond to the measurement processes for rows and for columns of the 2D signal, respectively.

of a 2D signal into sparse components and dense components, and apply CS only to sparse components using a smaller-sized sensing matrix. In [14] and [15], the statistical structure of the wavelet coefficients of a 2D image is considered for CS reconstruction of the image by using a scale mixture model. It is shown that fewer measurements are required in order to achieve a given reconstruction error performance. In addition, the scheme in [14] suggests to rearrange the wavelet coefficients into a new 2D matrix and sample each column of the matrix using the same sensing matrix  $\mathbf{A}$  of a smaller size.

All above research works focus on the encoder side, aiming at reducing the implementation cost and the storage and computational complexity of the encoder. Joint reconstruction is employed in these schemes, and thus, the complexity at the decoder side is still high.

Taking into account the implementation cost and the storage and computational complexity of the decoder, a block-based CS architecture can be employed in video compression where all blocks can be sampled and reconstructed independently. In [16] and [17], it is proposed to apply CS only to sparse blocks found by a block classification scheme that considers the difference of sparsity levels among different blocks in an image or a video frame. Another block classification scheme based on inter-frame correlation is proposed in [18].

In this paper, a parallel CS scheme is developed. A multidimensional sparse signal is considered, i.e., the signal is sparse in the identity basis. The multidimensional signal is first rearranged into a 2D matrix, and then sampled column-by-column via CS using the same sensing matrix. In this way, the required size of the sensing matrix can be reduced significantly compared to the scheme that samples the vectorized signal. Furthermore, both sampling and reconstruction can be conducted for individual columns in parallel. Note that several works use a similar column-by-column sampling setting at the encoder side, e.g., the aforementioned scheme of [14]. The focus of [14] is on studying the scale mixture models used in CS for image reconstruction. The signal considered in [14] is the matrix of wavelet coefficients. Another example is the multiple measurement vectors (MMV) model of [19], which considers a group of signals that share the same sparsity profile. In the MMV model, a group of signals are sampled using the same dictionary, which is analogous to the sensing matrix in CS, while the group of signals can be viewed as a virtual 2D signal. Joint reconstruction is then used for the MMV model. Compared to the aforementioned works [14] and [19], which consider some specific sparse signals and require joint reconstruction at the decoder side, we address a more general setting at the encoder side and develop a parallel reconstruction at the decoder side. Moreover, we derive some analytical results related to the parallel CS scheme. Although joint reconstruction of multiple vectors, e.g., reconstruction of multiple vectors via sum-of-norm minimization, can bring some benefits [20], it is shown that the uniform-recovery

rate in the sum-of-norm minimization case cannot exceed that for the case of individual reconstruction of each vector [21]. Besides, there are problems that cannot be solved by the joint recovery via sum-of-norm minimization, but can be solved by individually and independently reconstructing each vector [21].

In the parallel CS architecture proposed in this paper, a 2D signal may be permuted before it is sampled. It is because the permutation may provide benefits, for example, in computation and storage. Permutations are studied in several papers related to CS, though the goals of permutations in the existing literature are very different from our goal here. In [22], a segmented CS architecture is proposed and it is shown that a similar improvement to that obtained by increasing the size of the measurement matrix can be achieved by using a virtual extended measurement matrix obtained by permuting the existing rows of the initial measurement matrix. In [23], it is shown that if nonzero entries of a sparse signal are clustered, the deterministic Delsarte-Goethals frame used as sensing matrix does not work. Thus, it is proposed to apply permutations to the signal in order to avoid clustered nonzero entries. In our paper, the goal for applying permutations is different. Specifically, the parallel CS architecture considers sensing matrices that satisfy the RIP, and permutation is applied to 2D-reshaped signal aiming at ensuring that all columns of such signal have similar sparsity levels. We show that if a so-called acceptable permutation is conducted before sampling, the sensing matrix needs to satisfy the RIP of a smaller order than the sensing matrix of the parallel CS without any permutation. Thus, the storage and computational complexity can be further reduced. In our paper, a group-scan-based permutation is introduced for 2D signals which can be divided into a number of groups with elements in each group having the same probability to be large in magnitude. As a special case of such group-scan-based permutation, a zigzag-scan-based permutation is introduced and investigated for 2D signals satisfying a newly introduced layer model. A video compression scheme based on the proposed parallel CS with the zigzag-scan-based permutation is also developed and investigated. It improves the peak signal-to-noise ratio (PSNR) of reconstructed frames compared to parallel CS without permutation. This demonstrates the effectiveness of the zigzag-scan-based permutation in image compression.

In summary, this paper makes four main contributions. First, we propose a parallel CS scheme, which reduces the required size of sensing matrix and can be conducted at both the encoding and decoding sides in a parallel (column-by-column) manner. Second, we investigate properties of permutations when applied to parallel CS. Third, we introduce a group-scan-based permutation and a zigzag-scan-based permutation and as an example we show that the zigzag-scan-based permutation is an acceptable permutation with a large probability for 2D signals satisfying a newly introduced layer model. Finally, an application of the proposed parallel CS with the zigzag-scan-based permutation to video compression in wireless

multimedia sensor networks is discussed. Some very preliminary results have been reported in [24].

The remainder of the paper is organized as follows. Section II introduces the parallel CS scheme. Permutations are discussed in Section III. Section IV describes the video compression scheme that employs parallel CS with the zigzag-scan-based permutation in application to wireless multimedia sensor networks. Simulation results are given in Section V. Finally, conclusions are given in Section VI. The software needed to generate the numerical results can be obtained from <http://www.ualberta.ca/~hfang2/pub/2013TSP.zip>.

## II. PARALLEL CS

Given any multidimensional sparse signal, we can rearrange it into a 2D matrix  $\mathbf{X} \in \mathbb{R}^{M \times N}$ . A multidimensional signal and the corresponding 2D matrix  $\mathbf{X}$  are called  $s$ -sparse or have sparsity level  $s$  if  $\mathbf{X}$  has only  $s$  nonzero entries. The sparsity level of  $\mathbf{X}$  can be denoted as a sparsity vector  $\mathbf{s} = [s_1, s_2, \dots, s_N]$ , where  $s_j$  is the sparsity level of the  $j$ -th column of  $\mathbf{X}$ . In other words, the  $j$ -th column of  $\mathbf{X}$  has only  $s_j$  nonzero entries. Apparently,  $\|\mathbf{s}\|_1 = s$ .

In terms of the 2D signal  $\mathbf{X}$ , the proposed parallel CS consists of sampling each column of  $\mathbf{X}$  by the same sensing matrix  $\mathbf{A}$  and reconstructing these columns individually and in parallel by using any 1D CS reconstruction algorithm. In this paper, for presentation simplicity, we consider 2D signals, i.e., rearrangement of a multidimensional signal into a 2D matrix is done in advance.

### A. Theoretical Results on CS for 1D Signals

Most practical signals are not strictly sparse, but rather regarded as *compressible*, i.e., they have only a few large<sup>2</sup> elements. Here we use a 1D signal  $\mathbf{x}$  as an example. The signal  $\mathbf{x}$  can be approximated using its *best  $s$ -term approximation* denoted as  $\mathbf{x}^s$ , which is an  $s$ -sparse signal generated by keeping the  $s$  largest entries in  $\mathbf{x}$  and changing the remaining entries to zeros. The best  $s$ -term approximation is regarded as an optimal approximation using only  $s$  elements. However, such approximation requires knowledge about the values and locations of all elements in  $\mathbf{x}$ .

On the other hand, when CS is applied to  $\mathbf{x}$ , it is known that, if the sensing matrix  $\mathbf{A}$  obeys the RIP of order  $s$ , the reconstruction via solving (1) is nearly as good as that using the best  $s$ -term approximation, as shown in the following Lemma 1 [3], [25].

**Definition 1:** [3] For every integer  $s = 1, 2, \dots$ , the  $s$ -restricted isometry constant  $\delta_s$  of a given matrix  $\mathbf{A}$  is defined as the smallest quantity such that the inequality

$$(1 - \delta_s) \|\mathbf{z}\|_2^2 \leq \|\mathbf{Az}\|_2^2 \leq (1 + \delta_s) \|\mathbf{z}\|_2^2$$

<sup>2</sup>In this paper, when we say a value is large or small, it means the magnitude of the value is large or small.

holds for all sparse signals  $\mathbf{z}$  with no more than  $s$  nonzero entries, where  $\|\cdot\|_2$  denotes the  $\ell_2$ -norm of a vector.

**Lemma 1:** [25] Assume that  $\delta_{2s} < \sqrt{2} - 1$  for a sensing matrix  $\mathbf{A}$ . Then for a signal  $\mathbf{x}$ , the solution  $\mathbf{x}^*$  to (1) obeys

$$\begin{aligned} \|\mathbf{x}^* - \mathbf{x}\|_1 &\leq G \cdot \|\mathbf{x} - \mathbf{x}^s\|_1 \quad \text{and} \\ \|\mathbf{x}^* - \mathbf{x}\|_2 &\leq G' \cdot \|\mathbf{x} - \mathbf{x}^s\|_1 / \sqrt{s} \end{aligned} \quad (2)$$

for some constants  $G$  and  $G'$ .

In this paper, if the RIP condition holds for  $\mathbf{A}$  with  $\delta_{2s} < \sqrt{2} - 1$ , the matrix  $\mathbf{A}$  is regarded as obeying the RIP of order  $s$ . Therefore, according to Lemma 1, an  $s$ -sparse signal can be exactly reconstructed via solving (1) if the sensing matrix  $\mathbf{A}$  obeys the RIP of order  $s$ . For a compressible signal  $\mathbf{x}$ , if a sensing matrix  $\mathbf{A}$  obeying the RIP of order  $s$  is used to sample  $\mathbf{x}$ , the reconstruction via solving (1) has an error bounded by the  $\ell_1$ -norm of the approximation error when  $\mathbf{x}^s$  is used to approximate  $\mathbf{x}$ . Note that, for reconstruction via solving (1), we do not need knowledge about the values and locations of all elements in  $\mathbf{x}$ , while such knowledge is needed if  $\mathbf{x}^s$  is used to approximate  $\mathbf{x}$ .

### B. New Theoretical Results on Parallel CS for 2D Signals

Based on Lemma 1, the following lemma gives a sufficient condition for exact reconstruction of a 2D  $s$ -sparse signal using parallel CS.

**Lemma 2:** Consider a 2D  $s$ -sparse signal  $\mathbf{X}$  with sparsity vector  $\mathbf{s}$ , if the RIP of order  $\|\mathbf{s}\|_\infty$  holds for the sensing matrix  $\mathbf{A}$ , i.e.,  $\delta_{2\|\mathbf{s}\|_\infty} < \sqrt{2} - 1$ , where  $\|\cdot\|_\infty$  stands for the Chebyshev norm of a vector<sup>3</sup>, then  $\mathbf{X}$  can be exactly reconstructed using parallel CS scheme.

*Proof:* The proof follows the same steps as the proof for the following Lemma 3. ■

For a 2D compressible signal  $\mathbf{X}$ , the following lemma gives a sufficient condition that the reconstruction error of the parallel CS is bounded by the  $\ell_1$ -norm of the approximation error when the best  $s$ -term approximation of  $\mathbf{X}$ , denoted as  $\mathbf{X}^s$ , is used to approximate  $\mathbf{X}$ .

**Lemma 3:** Let  $\mathbf{X}^s \in \mathbb{R}^{M \times N}$ , which has a sparsity vector  $\mathbf{s} = [s_1, s_2, \dots, s_N]$ , be the best  $s$ -term approximation of  $\mathbf{X} \in \mathbb{R}^{M \times N}$ . If the sensing matrix  $\mathbf{A}$  obeys the RIP of order  $\|\mathbf{s}\|_\infty$ , i.e.,  $\delta_{2\|\mathbf{s}\|_\infty} < \sqrt{2} - 1$ , then the signal  $\hat{\mathbf{X}}$  reconstructed using parallel CS scheme obeys

$$\|\hat{\mathbf{X}} - \mathbf{X}\|_1 \leq G \cdot \|\mathbf{X} - \mathbf{X}^s\|_1 \quad \text{and}$$

<sup>3</sup>The Chebyshev norm of a vector is equal to the largest magnitude of the elements in the vector.



$$\|\hat{\mathbf{X}} - \mathbf{X}\|_2 \leq G' \cdot \|\mathbf{X} - \mathbf{X}^s\|_1 \quad (3)$$

where  $G$  and  $G'$  are finite constants.

*Proof:* Since for all  $1 \leq j \leq N$ ,  $\|\mathbf{s}\|_\infty \geq s_j$ , and according to the definition of  $s$ -restricted isometry constant, we have  $\delta_{2s_j} \leq \delta_{2\|\mathbf{s}\|_\infty} < \sqrt{2} - 1$ . Then, according to (2), we obtain that

$$\|\hat{\mathbf{x}}_j - \mathbf{x}_j\|_1 \leq G_j \cdot \|\mathbf{x}_j - \mathbf{x}_j^s\|_1$$

and

$$\|\hat{\mathbf{x}}_j - \mathbf{x}_j\|_2 \leq G'_j \cdot \|\mathbf{x}_j - \mathbf{x}_j^s\|_1 \cdot s_j^{-1/2}$$

where  $\mathbf{x}_j$ ,  $\hat{\mathbf{x}}_j$ , and  $\mathbf{x}_j^s$  denote the  $j$ -th column of  $\mathbf{X}$ ,  $\hat{\mathbf{X}}$ , and  $\mathbf{X}^s$ , respectively, and  $G_j$  and  $G'_j$  are finite constants. Therefore, by choosing  $G = \max_j\{G_j\}$  and  $G' = \max_j\{G'_j\}$ , we obtain that

$$\begin{aligned} \|\hat{\mathbf{X}} - \mathbf{X}\|_1 &= \sum_{i=1}^N \|\hat{\mathbf{x}}_i - \mathbf{x}_i\|_1 \\ &\leq G \cdot \sum_{j=1}^N \|\mathbf{x}_j - \mathbf{x}_j^s\|_1 = G \cdot \|\mathbf{X} - \mathbf{X}^s\|_1 \end{aligned}$$

and

$$\begin{aligned} \|\hat{\mathbf{X}} - \mathbf{X}\|_2 &= \sqrt{\sum_{j=1}^N \|\hat{\mathbf{x}}_j - \mathbf{x}_j\|_2^2} \\ &\leq \sqrt{G'^2 \cdot \sum_{i=1}^N \|\mathbf{x}_i - \mathbf{x}_i^s\|_1^2} = G' \cdot \sqrt{\sum_{j=1}^N \|\mathbf{x}_j - \mathbf{x}_j^s\|_1^2} \\ &\leq G' \cdot \sum_{j=1}^N \|\mathbf{x}_j - \mathbf{x}_j^s\|_1 = G' \cdot \|\mathbf{X} - \mathbf{X}^s\|_1. \end{aligned}$$

This completes the proof. ■

To sum up, for parallel CS, the RIP condition for the sensing matrix  $\mathbf{A}$  for a given reconstruction quality is related to  $\|\mathbf{s}\|_\infty$ . In Subsection III-A, it will be shown that the RIP condition can be relaxed by performing a so-called acceptable permutation before using the parallel CS.

### III. PERMUTATION

When parallel CS is applied to a 2D compressible signal<sup>4</sup>  $\mathbf{X}$ , the difference of sparsity levels among columns of  $\mathbf{X}^s$  (which has sparsity vector  $\mathbf{s}$ ) is not considered, and thus, the ‘worst-case’ sparsity level of the columns of  $\mathbf{X}^s$ , i.e.,  $\|\mathbf{s}\|_\infty$ , needs to be taken into account when designing the sensing matrix. In this section, permutation is introduced such that by permuting<sup>5</sup> entries of  $\mathbf{X}$  all columns of the best  $s$ -term approximation of the newly formed 2D signal would share similar sparsity levels.

<sup>4</sup>Without loss of generality, compressible signals are considered in the remainder of the paper, since a sparse signal can be regarded as a special case of a compressible signal.

<sup>5</sup>In this paper, when we say “permute”, it means exchanging entries in a 2D matrix, while not changing the dimension of the matrix.



Let  $\mathbf{P}(\cdot)$  be a permutation operator which maps a matrix into another matrix by permuting its elements and  $\mathbf{P}^{-1}(\cdot)$  be the corresponding inverse permutation operator. Then  $\mathbf{X}^\dagger = \mathbf{P}(\mathbf{X})$  and  $\mathbf{X} = \mathbf{P}^{-1}(\mathbf{X}^\dagger)$  where  $\mathbf{X}^\dagger \in \mathbb{R}^{M \times N}$  is a permuted 2D signal.

With permutation before sampling, the parallel sampling process can be described as follows

$$\mathbf{y}_j = \mathbf{A}\mathbf{x}_j^\dagger \quad (4)$$

where  $\mathbf{x}_j^\dagger$  is the  $j$ -th column of  $\mathbf{X}^\dagger$ , and  $\mathbf{y}_j$  is the measurement vector of  $\mathbf{x}_j^\dagger$ . We can rewrite (4) in the matrix form as

$$\mathbf{Y} = \mathbf{A}\mathbf{X}^\dagger = \mathbf{A}\mathbf{P}(\mathbf{X}) \quad (5)$$

where  $\mathbf{Y} = [\mathbf{y}_1, \mathbf{y}_2, \dots, \mathbf{y}_N]$ .

For signal reconstruction, all columns of  $\mathbf{X}^\dagger$  can be reconstructed in parallel by any existing CS reconstruction algorithm. Let  $\hat{\mathbf{X}}^\dagger$  be the reconstructed permuted signal. Then we can apply inverse permutation to  $\hat{\mathbf{X}}^\dagger$  to obtain the reconstructed 2D signal  $\hat{\mathbf{X}}$ , that is,

$$\hat{\mathbf{X}} = \mathbf{P}^{-1}(\hat{\mathbf{X}}^\dagger). \quad (6)$$

#### A. Discussion about Permutation

For any multidimensional signal, the permutation can be either applied after or included in the process of rearranging the multidimensional signal into a 2D matrix. The block-based CS employed in [8], [9] and [17] is a special case of the parallel CS, which can be interpreted as making each vectorized block as a column of a new 2D signal. Furthermore, the problem of difference of sparsity levels among blocks is addressed in [17] by employing a classification scheme to identify sparse blocks and dense blocks and then applying CS only to the sparse blocks. In our work, permutation is applied to a 2D compressible signal  $\mathbf{X}$  or integrated into the process of rearrangement of a multidimensional signal to a 2D compressible signal  $\mathbf{X}$  such that all columns of  $\mathbf{X}^{\dagger s}$  (the best  $s$ -term approximation of the resulted 2D signal  $\mathbf{X}^\dagger$ ) are sparse. Thus, the classification step of [17] is avoided.

Consider a compressible 2D signal  $\mathbf{X}$  and its best  $s$ -term approximation  $\mathbf{X}^s$  with sparsity vector  $\mathbf{s}$  (then we have  $\|\mathbf{s}\|_1 = s$ ). If the sensing matrix  $\mathbf{A} \in \mathbb{R}^{K \times M}$  is constructed from Gaussian ensembles with

$$K \geq C \cdot \|\mathbf{s}\|_\infty \log(M/\|\mathbf{s}\|_\infty) \quad (7)$$

for some constant  $C$ , then it will satisfy the RIP of order  $\|\mathbf{s}\|_\infty$  [3]. Then according to Lemma 3, the signal  $\hat{\mathbf{X}}$  reconstructed using parallel CS obeys (3).

**Definition 2:** For a 2D compressible signal  $\mathbf{X} \in \mathbb{R}^{M \times N}$  and its best  $s$ -term approximation  $\mathbf{X}^s$  with sparsity vector  $\mathbf{s}$ , a permutation  $P(\cdot)$  is called acceptable for  $\mathbf{X}$  if the Chebyshev norm of the sparsity vector of the best  $s$ -term approximation of the signal  $P(\mathbf{X})$  is smaller than  $\|\mathbf{s}\|_\infty$ .

When permutation is applied before parallel CS, the signal after permutation is  $\mathbf{X}^\dagger$ , and the best  $s$ -term approximation of  $\mathbf{X}^\dagger$  is denoted as  $\mathbf{X}^{\dagger s}$  with sparsity vector  $\mathbf{s}^\dagger$  (then we have  $\|\mathbf{s}^\dagger\|_1 = s$ ). Consider that  $M \gg \|\mathbf{s}\|_\infty$  and  $M \gg \|\mathbf{s}^\dagger\|_\infty$ , i.e.,  $\mathbf{X}^s$  and  $\mathbf{X}^{\dagger s}$  are sparse enough. If  $\|\mathbf{s}^\dagger\|_\infty < \|\mathbf{s}\|_\infty$ , it can be seen that for parallel CS with an acceptable permutation, the lower bound of  $K$  in (7) is smaller than that in parallel CS without an acceptable permutation. In other words, for the sufficient condition in Lemmas 2 and 3, the condition “ $\mathbf{A}$  obeys the RIP of order  $\|\mathbf{s}^\dagger\|_\infty$ ” for parallel CS with an acceptable permutation is weaker than the condition “ $\mathbf{A}$  obeys the RIP of order  $\|\mathbf{s}\|_\infty$ ” for parallel CS without an acceptable permutation. To sum up, the RIP condition for a given reconstruction quality is weaker after permutation if  $\|\mathbf{s}^\dagger\|_\infty$  is smaller than  $\|\mathbf{s}\|_\infty$ .

Since  $\|\mathbf{s}^\dagger\|_1 = \|\mathbf{s}\|_1 = s$ , it is desired that, after an acceptable permutation, the  $s$  nonzero elements in the best  $s$ -term approximation of the permuted 2D signal are evenly distributed among the columns, which leads to minimum  $\|\mathbf{s}^\dagger\|_\infty$ . Such a permutation is an optimal permutation defined below.

**Definition 3:** For a 2D compressible signal  $\mathbf{X} \in \mathbb{R}^{M \times N}$  and its best  $s$ -term approximation  $\mathbf{X}^s$ , if after a permutation, the best  $s$ -term approximation  $\mathbf{X}^{\dagger s}$  of the resulted 2D signal  $\mathbf{X}^\dagger$  has sparsity vector  $\mathbf{s}^*$  satisfying  $\max_i \{s_i^*\} - \min_i \{s_i^*\} \leq 1$ , where  $s_i^*$  denotes the  $i$ -th entry of  $\mathbf{s}^*$ , then  $\mathbf{s}^*$  is called an optimal sparsity vector of  $\mathbf{X}^s$ , and the corresponding permutation is called an optimal permutation of  $\mathbf{X}$ .

**Lemma 4:** For a 2D compressible signal  $\mathbf{X} \in \mathbb{R}^{M \times N}$  and its best  $s$ -term approximation  $\mathbf{X}^s$ , there exists at least one optimal sparsity vector  $\mathbf{s}^*$  of  $\mathbf{X}^s$ .

*Proof:* Obviously,  $\|\mathbf{s}^*\|_1 = s$ . If  $\lceil s/N \rceil = \lfloor s/N \rfloor = s/N$  (where  $\lceil \cdot \rceil$  denotes the ceiling function and  $\lfloor \cdot \rfloor$  denotes the floor function), we can immediately find an optimal sparsity vector  $\mathbf{s}^*$  whose entries are all  $s/N$ . If  $\lceil s/N \rceil \neq \lfloor s/N \rfloor$ , we consider a permutation on  $\mathbf{X}$  such that: for the best  $s$ -term approximation of the resulted 2D signal, there are  $\lceil s/N \rceil$  nonzero elements in each of the first  $s - N\lfloor s/N \rfloor$  columns, and the remaining nonzero elements are evenly distributed among the remaining columns. Then each of the last  $N\lfloor s/N \rfloor - s$  columns has  $\lfloor s/N \rfloor$  nonzero entries. Therefore, the sparsity vector of the best  $s$ -term approximation of the permuted 2D signal is an optimal sparsity vector. This completes the proof. ■

From the proof of Lemma 4, it follows that optimal sparsity vector and optimal permutation may not be unique, and the Chebyshev norm of an optimal sparsity vector of  $\mathbf{X}^s$  is equal to  $\lceil s/N \rceil$ .

In most scenarios, finding an optimal permutation may not be practical. An acceptable permutation defined in Definition 2 can be used instead.

### B. Group-scan-based Permutation and Zigzag-scan-based Permutation

The following observation is of interest. For a 2D compressible signal  $\mathbf{X} \in \mathbb{R}^{M \times N}$ , consider a permuted signal  $\mathbf{X}^\dagger$  and its best  $s$ -term approximation  $\mathbf{X}^{\dagger s}$ . For any  $1 \leq i \leq N$ , if all elements in the  $i$ -th row of  $\mathbf{X}^{\dagger s}$  share the same probability to be nonzero, denoted as  $p_i$ , then all columns of  $\mathbf{X}^{\dagger s}$  have the same expected sparsity level, given as  $\sum_{i=1}^M p_i$ .

For example, when  $M = N = 4$ , if after a permutation, the elements in the 1st, 2nd, 3rd and 4th rows of  $\mathbf{X}^{\dagger s}$  have respectively probabilities  $p_1 = 0.9$ ,  $p_2 = 0.3$ ,  $p_3 = 0.2$  and  $p_4 = 0.1$  to be nonzero, then for the sparsity vector of  $\mathbf{X}^{\dagger s}$ , denoted as  $\mathbf{s}^\dagger = [s_1^\dagger, s_2^\dagger, s_3^\dagger, s_4^\dagger]$ , we have

$$E \left\{ \max_j \{s_j^\dagger\} - \min_j \{s_j^\dagger\} \right\} = 1.3881$$

and

$$\Pr \left\{ \max_j \{s_j^\dagger\} - \min_j \{s_j^\dagger\} \leq 1 \right\} = 0.6003 \quad (8)$$

where  $E\{\cdot\}$  means expectation and  $\Pr\{\cdot\}$  means probability of an event. Thus, the permutation in this example is optimal with probability 0.6003.

For the best  $s$ -term approximation  $\mathbf{X}^s$  of a 2D compressible signal  $\mathbf{X} \in \mathbb{R}^{M \times N}$ , consider that elements in  $\mathbf{X}^s$  can be divided into several non-overlapped groups, and in each group all elements share the same probability to be nonzero. Based on the observation at the beginning of this subsection, a permutation, named *group-scan-based permutation*, can work as follows: 1) preform group-by-group scan<sup>6</sup> of the 2D compressible signal  $\mathbf{X}$  into a vector, and 2) row-wisely reshape the resulted vector into a new  $M \times N$  2D signal. In this way, all columns of the best  $s$ -term approximation of the new 2D signal are likely to have similar sparsity levels.

**Definition 4:** For a 2D signal  $\mathbf{X} \in \mathbb{R}^{M \times N}$ , let  $\mathbf{X}(i, j)$  denote the element in the position  $(i, j)$ . The  $m$ -th ( $1 \leq m < M + N$ ) layer of  $\mathbf{X}$  is the group of all elements  $\mathbf{X}(i, j)$ 's satisfying  $i + j - 1 = m$ .

<sup>6</sup>That is, first scan all elements in the first group, then scan all elements in the second group, ..., and so on.

For example, when  $M = N = 4$ , the following matrix  $\mathbf{X}$

$$\mathbf{X} = \begin{bmatrix} x_1 & x_2 & x_6 & x_7 \\ x_3 & x_5 & x_8 & x_{13} \\ x_4 & x_9 & x_{12} & x_{14} \\ x_{10} & x_{11} & x_{15} & x_{16} \end{bmatrix} \quad (9)$$

has 7 layers, including  $\{x_1\}$ ,  $\{x_2, x_3\}$ ,  $\{x_4, x_5, x_6\}$ ,  $\{x_7, x_8, x_9, x_{10}\}$ ,  $\{x_{11}, x_{12}, x_{13}\}$ ,  $\{x_{14}, x_{15}\}$ ,  $\{x_{16}\}$ , respectively. The layers of  $\mathbf{X}$  are parallel to each other.

For a 2D compressible signal  $\mathbf{X}$ , if elements in each layer of its best  $s$ -term approximation  $\mathbf{X}^s$  have similar probabilities to be nonzero (an example when this condition is satisfied is to be given later in this subsection), then we propose the following zigzag-scan-based permutation, which is a special example of the group-scan-based permutation.

Define the *zigzag-scan-based permutation*  $\mathbf{P}: \mathbb{R}^{M \times N} \rightarrow \mathbb{R}^{M \times N}$  for a 2D signal  $\mathbf{X} \in \mathbb{R}^{M \times N}$  as  $\mathbf{P}(\mathbf{X}) = \mathbf{R}(\mathbf{Z}(\mathbf{X}))$ , where  $\mathbf{R}: \mathbb{R}^{MN} \rightarrow \mathbb{R}^{M \times N}$  is the row-wisely reshaping function which row-wisely turns a vector into an  $M \times N$  matrix and  $\mathbf{Z}: \mathbb{R}^{M \times N} \rightarrow \mathbb{R}^{MN}$  is the zigzag scan function which turns a matrix into a “zigzag” sequence vector.

Correspondingly, define the *inverse zigzag-scan-based permutation*  $\mathbf{P}^{-1}: \mathbb{R}^{M \times N} \rightarrow \mathbb{R}^{M \times N}$  for a 2D signal  $\mathbf{X}^\dagger \in \mathbb{R}^{M \times N}$  as  $\mathbf{P}^{-1}(\mathbf{X}^\dagger) = \mathbf{Z}^{-1}(\mathbf{R}^{-1}(\mathbf{X}^\dagger))$ , where  $\mathbf{R}^{-1}: \mathbb{R}^{M \times N} \rightarrow \mathbb{R}^{MN}$  is a vectorization function which row-wisely turns a matrix into a vector and  $\mathbf{Z}^{-1}: \mathbb{R}^{MN} \rightarrow \mathbb{R}^{M \times N}$  is inverse zigzag scan function which turns a “zigzag” sequence into an  $M \times N$  matrix.

For example, the matrix  $\mathbf{X}$  given in (9) becomes a “zigzag” sequence after zigzag scan, i.e.,

$$\mathbf{Z}(\mathbf{X}) = [x_1, x_2, x_3, x_4, x_5, x_6, x_7, \dots, x_{16}],$$

and then becomes the permuted signal  $\mathbf{X}^\dagger$  after row-wisely reshaping, that is,

$$\begin{aligned} \mathbf{X}^\dagger &= \mathbf{P}(\mathbf{X}) = \mathbf{R}(\mathbf{Z}(\mathbf{X})) \\ &= \mathbf{R}([x_1, x_2, x_3, x_4, x_5, x_6, x_7, \dots, x_{16}]) \\ &= \begin{bmatrix} x_1 & x_2 & x_3 & x_4 \\ x_5 & x_6 & x_7 & x_8 \\ x_9 & x_{10} & x_{11} & x_{12} \\ x_{13} & x_{14} & x_{15} & x_{16} \end{bmatrix}, \end{aligned}$$

and again becomes a “zigzag” sequence after vectorization, that is,

$$\mathbf{R}^{-1}(\mathbf{X}^\dagger) = \mathbf{Z}(\mathbf{X}) = [x_1, x_2, x_3, x_4, x_5, x_6, x_7, \dots, x_{16}],$$

and then returns to the original signal  $\mathbf{X}$  after inverse zigzag scan, i.e.,  $\mathbf{P}^{-1}(\mathbf{X}^\dagger) = \mathbf{Z}^{-1}(\mathbf{R}^{-1}(\mathbf{X}^\dagger)) = \mathbf{X}$ .

Thus, according to the analysis at the beginning of this subsection, if elements in each layer of  $\mathbf{X}^s$  share similar probabilities to be nonzero, after the zigzag-scan-based permutation, all columns of the permuted  $\mathbf{X}^s$  tend to have similar sparsity levels.

**Definition 5:** Consider a 2D compressible signal  $\mathbf{X} \in \mathbb{R}^{M \times N}$  and its best  $s$ -term approximation  $\mathbf{X}^s$ . For given transition layer indices  $r_0, r_1, r_2$  and a decay factor  $\alpha$ , we say that  $\mathbf{X}$  follows the  $(r_0, r_1, r_2, \alpha)$ -layer model if the probability of the event  $E_m$  that an element in the  $m$ -th layer of  $\mathbf{X}^s$  is nonzero follows the probability distribution

$$\Pr \{E_m\} = \begin{cases} 0 & 1 \leq m \leq r_0 \\ 1 & r_0 + 1 \leq m \leq r_1 \\ e^{-\alpha(m-r_0)} & r_1 + 1 \leq m \leq r_2 \\ 0 & r_2 + 1 \leq m \leq M + N - 1. \end{cases}$$

Based on the  $(r_0, r_1, r_2, \alpha)$ -layer model, we have the following proposition for the zigzag-scan-based permutation.

**Proposition 1:** If a 2D compressible signal  $\mathbf{X} \in \mathbb{R}^{M \times N}$  follows the  $(r_0, r_1, r_2, \alpha)$ -layer model with  $r_2 \geq 2r_1 - 3r_0 - 1$  and  $0 \leq r_0 < r_1 < r_2 \leq \min\{M, N\}$ , the zigzag-scan-based permutation  $P(\cdot)$  is an acceptable permutation with a large probability that is given as

$$\begin{aligned} \Pr \{\mathbf{P} \text{ is acceptable}\} &= \Pr \left\{ \|\mathbf{s}\|_\infty > \|\mathbf{s}^\dagger\|_\infty \right\} \\ &\geq 1 - \left[ \prod_{m=r_1+1}^{r_2} (1 - p_m)^m \right] \cdot \prod_{j=1}^{r_2} \left\{ 1 + \sum_{k=k_j+1}^{\min\{[(r_0+r_2+1)/2], r_2-r_0, r_2-j+1\}} \right. \\ &\quad \left. \sum_{\substack{a_1, a_2, \dots, a_{k-k_j} \in \mathcal{A}_j \\ a_1 < a_2 < \dots < a_{k-k_j}}} \frac{1}{(e^{\alpha(a_1-1-r_0)} - 1) \dots (e^{\alpha(a_{k-k_j}-1-r_0)} - 1)} \right\} \end{aligned} \quad (10)$$

where  $\mathbf{s}$  and  $\mathbf{s}^\dagger$  are the sparsity vectors of the best  $s$ -term approximation of  $\mathbf{X}$  and  $\mathbf{X}^\dagger$ , respectively,  $\mathbf{X}^\dagger$  is a 2D signal after the zigzag-scan-based permutation, and for  $1 \leq j \leq r_2$ ,  $\mathcal{A}_j \triangleq \{m_j, m_j + 1, \dots, r_2\}$ ,  $m_j = \max\{r_1 + 1, j\}$ , and

$$k_j = \begin{cases} r_1 - r_0, & 1 \leq j \leq r_0 \\ r_1 - j + 1, & r_0 + 1 \leq j \leq r_1 \\ 0, & r_1 + 1 \leq j \leq r_2. \end{cases}$$

*Proof:* See Appendix for the proof. ■

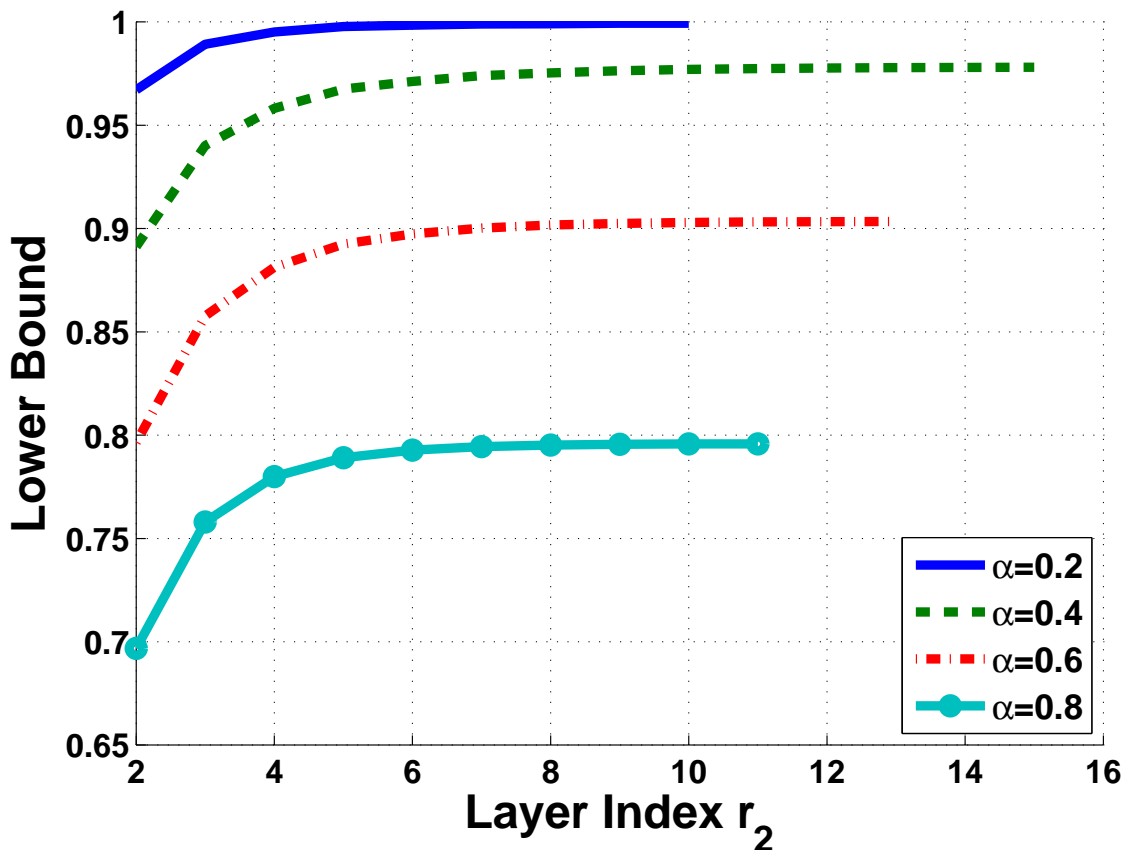


Fig. 1: Lower bound of  $\Pr\{\text{P is acceptable}\}$  in (10) for  $r_0 = 0, r_1 = 1$ .

Figs. 1–3 show the value of the lower bound on  $\Pr\{\text{P is acceptable}\}$  in (10) under different  $\alpha$  and  $r_2$  for 1)  $r_0 = 0, r_1 = 1$ ; 2)  $r_0 = 0, r_1 = 2$ ; and 3)  $r_0 = 3, r_1 = 5$ . It can be seen that the lower bound on  $\Pr\{\text{P is acceptable}\}$  is large enough in general. For other  $r_0$  and  $r_1$ , the results are similar.

From Proposition 1, it can be seen that the zigzag-scan-based permutation is an acceptable permutation for a very broad class of signals. The knowledge of exact locations of the nonzero entries of the best  $s$ -term approximation  $\mathbf{X}^s$ , i.e., the knowledge of the support of the 2D signal  $\mathbf{X}^s$ , is not needed.

As an example, we show that the zigzag-scan-based permutation is particularly useful for 2D discrete cosine transform (DCT2) coefficient matrices of 2D piecewise smooth image signals. Since the DCT2 coefficient matrix of a piecewise smooth image signal typically has most of its large elements lie in the top left corner, and small elements lie in the bottom right corner because most of its energy is concentrated in low frequencies, the zigzag scan process is commonly used in image compression like JPEG [26].

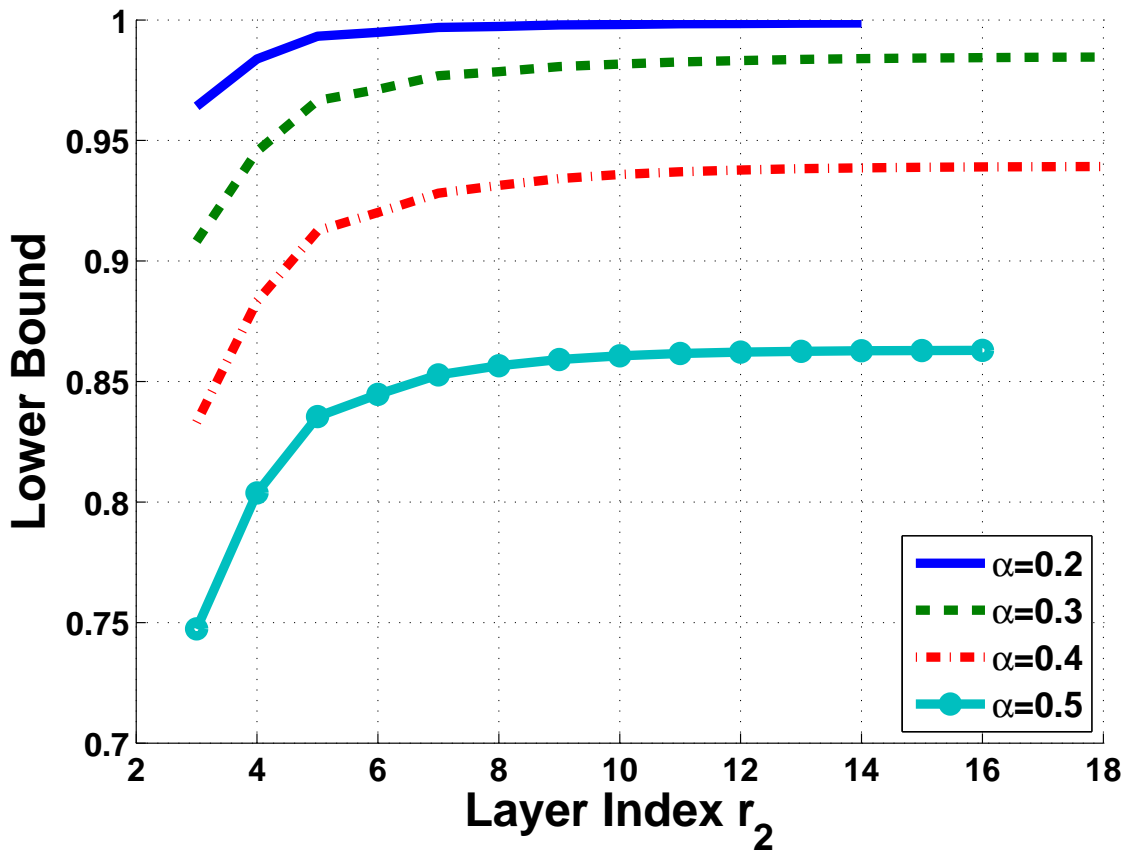


Fig. 2: Lower bound of  $\Pr \{P \text{ is acceptable}\}$  in (10) for  $r_0 = 0, r_1 = 2$ .

Thus, the DCT2 coefficient matrices of piecewise smooth image signals satisfy the  $(r_0, r_1, r_2, \alpha)$ -layer model with  $r_0 = 0$  (which will also be shown via simulation in Subsection V-A), and thus, the proposed zigzag-scan-based permutation has a large probability to be an acceptable permutation when parallel CS is applied to the DCT2 coefficient matrices. Note that the knowledge of the layer indices  $r_1, r_2$  and the decay factor  $\alpha$  of the layer model is not needed when applying the zigzag-scan-based permutation to the DCT2 coefficient matrices.

Fig. 4 shows the difference before and after the zigzag-scan-based permutation when the 2D signal is the DCT2 coefficient matrix of an image. The energy, which can be loosely viewed as an interpretation of the sparsity vector, if all non-zero entries of the 2D signal have magnitude of the same order, is distributed more evenly among columns after the zigzag-scan-based permutation.

One advantage of the zigzag-scan-based permutation is that it is a pre-defined permutation, and thus,



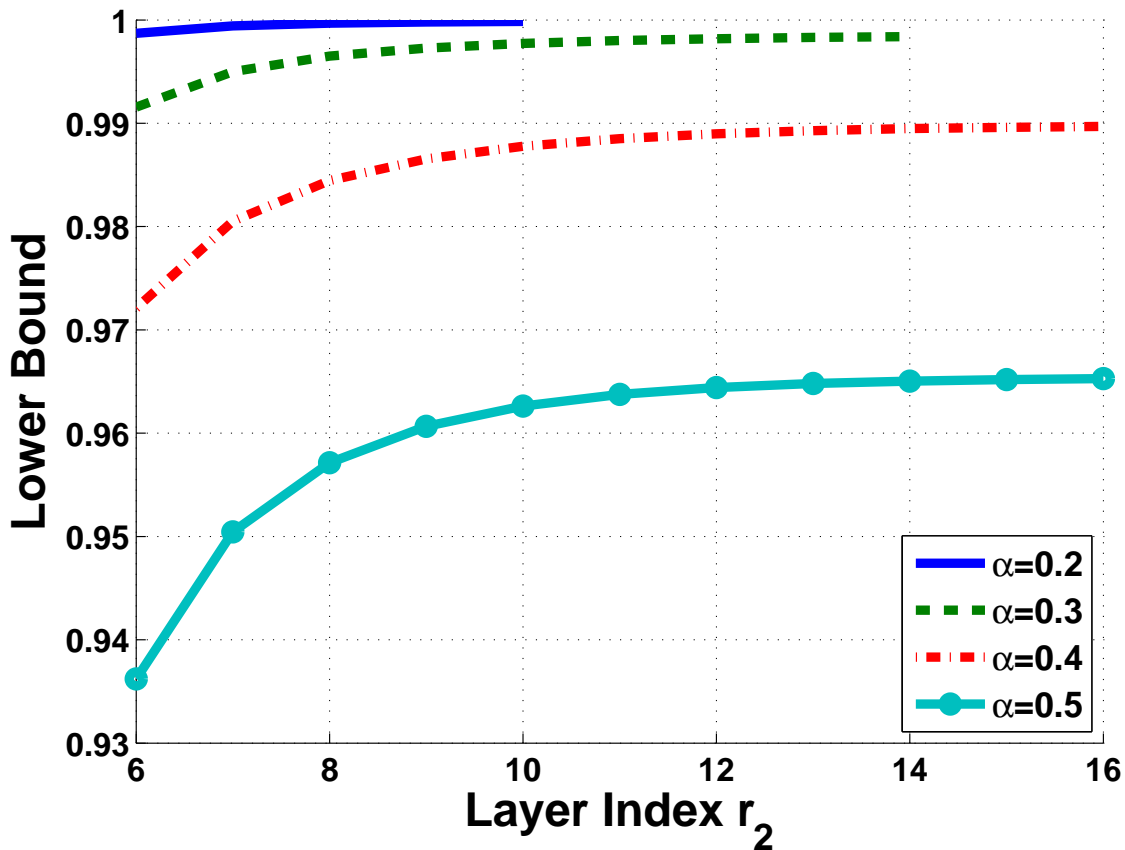


Fig. 3: Lower bound of  $\Pr\{P \text{ is acceptable}\}$  in (10) for  $r_0 = 3, r_1 = 5$ .

the encoder and decoder know it in advance without any additional communication. In Subsection V-A, we will also show by simulation that the zigzag-scan-based permutation is an acceptable permutation for DCT2 coefficient matrices of several typical images.

#### IV. EXAMPLE OF VIDEO COMPRESSION VIA PARALLEL CS WITH PERMUTATIONS IN WIRELESS MULTIMEDIA SENSOR NETWORKS

As an application example, we design a pair of CS video encoder and decoder based on parallel CS with the zigzag-scan-based permutation. This CS video encoder and decoder can be plugged into the application layer of the compressive distortion minimizing rate control (C-DMRC) system [27]. In wireless multimedia sensor networks, the C-DMRC system is preferred compared to traditional video coding standards such as MPEG, H.264, since the C-DMRC system has less-complex video encoder and can tolerate much higher bit error rates. The CS video encoder and decoder in the C-DMRC system are

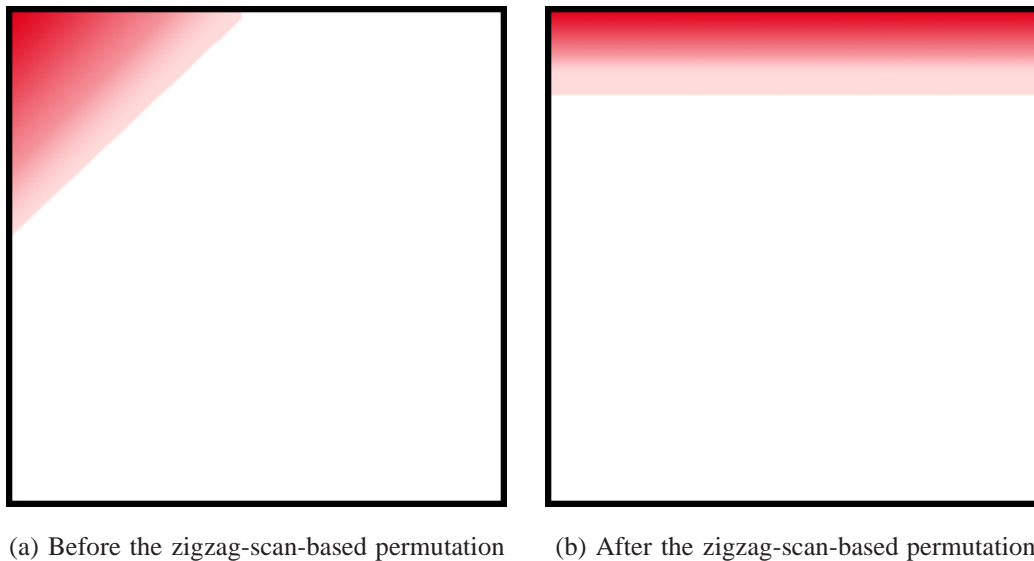
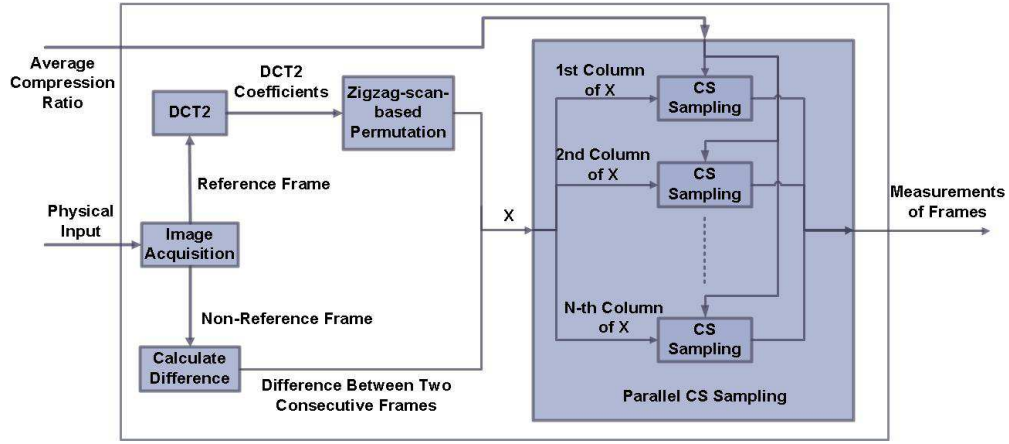


Fig. 4: Energy distribution of a DCT2 coefficient matrix before and after the zigzag-scan-based permutation.

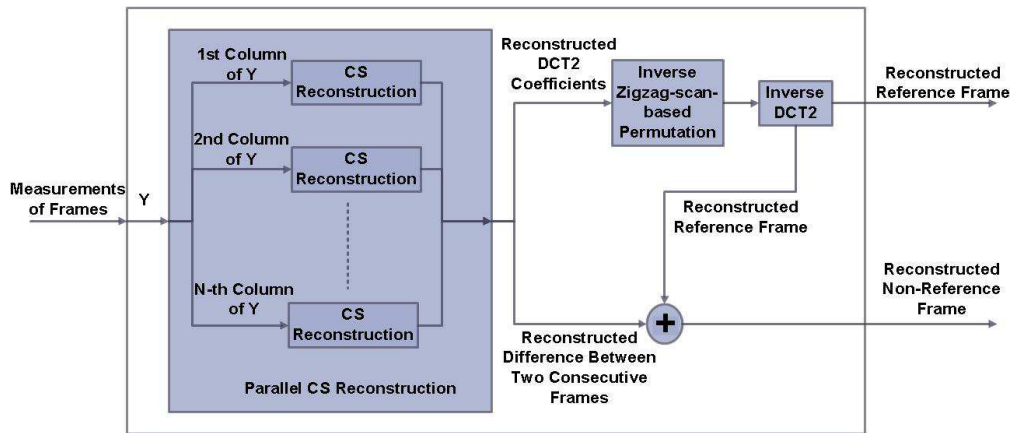
built based on the block CS architecture proposed in [10]. Thus, as we discussed in Section I, the CS video decoder in the C-DMRC system requires a joint reconstruction. By replacing the CS video encoder and decoder at the application layer of the C-DMRC system with the CS video encoder and decoder based on parallel CS architecture, the computational complexity of the video decoder can be reduced and the reconstruction process can be parallelized.

In this example, frames with odd indices and even indices are taken as reference frames and non-reference frames, respectively<sup>7</sup>. The block diagram of the CS video encoder is shown in Fig.5a. The average compression ratio is computed by the rate controller at the transport layer according to current network status (e.g., the end-to-end round trip time and the estimated sample loss rate of the network), and it controls the number of measurements for a video frame. For every pair of a reference frame and its following non-reference frame, the rate controller gives an average compression ratio. According to this average compression ratio, the compression ratios of the reference and non-reference frames in a pair are obtained. At the output of the CS video encoder we have the frame measurements. The image acquisition device turns the physical input into video frames and outputs the video frames to different processing blocks according to the frame index.

<sup>7</sup>More sophisticated index assignment schemes for the reference frame and non-reference frame can be used as well.



(a) Block diagram of the CS video encoder.



(b) Block diagram of the CS video decoder.

Fig. 5: Block diagram of the CS video encoder and decoder.

The procedure for encoding the reference frame is as follows: 1) compute DCT2 on the reference frame; 2) perform the zigzag-scan-based permutation on the DCT2 coefficient matrix; 3) perform parallel compressed sampling of the permuted DCT2 coefficient matrix. The procedure for encoding the non-reference frame is as follows: 1) compute the difference between the non-reference frame and the preceding reference frame; 2) perform parallel compressed sampling of this difference. The outputs of all CS sampling processors are combined.<sup>8</sup> For the non-reference frames, no permutation is performed since the difference between two consecutive frames, especially in videos with slow motion, is sparse enough so that the sparsity level of each column is too small to have significant difference from column

<sup>8</sup>Quantization is omitted in the example presented here, but it has to be done in a practical video coding scenario.

to column. Thus, the permutation does not bring significant improvement, which we have checked by simulations in [24].

Considering that the sparsity level of the difference between a non-reference frame and its preceding reference frame is smaller than that of the DCT2 coefficient matrix of the reference frame, the compression ratio of the non-reference frames should be higher than that of the reference frames, i.e., fewer measurements are assigned to the non-reference frames. In our experiment in Section V, we set the ratio of measurements being 4:1, i.e., the number of measurements for reference frames is 4 times that for non-reference frames. For example, if current average compression ratio given by the rate controller is 0.5, then the compression ratio of the reference frame is 0.8 and the compression ratio of the non-reference frame is 0.2. Other ratios can be set according to the motion intensity of the video.

The block diagram of the CS video decoder is shown in Fig. 5b. To decode a reference frame at the receiver side, the following steps are performed: 1) perform parallel CS reconstruction of the permuted DCT2 coefficient matrix from the measurements of the reference frame; 2) perform the inverse zigzag-scan-based permutation on the reconstructed permuted DCT2 coefficient matrix; 3) perform inverse DCT2 on the reconstructed DCT2 coefficient matrix. To decode a non-reference frame, the following steps are performed: 1) perform parallel CS reconstruction of the difference between the non-reference frame and its preceding reference frame from the measurements of the non-reference frame; 2) add the reconstructed difference between the non-reference frame and its preceding reference frame to the corresponding reconstructed reference frame. For parallel CS reconstruction, any  $\ell_1$ -norm minimization solver, e.g., the basis pursuit algorithm, can be used.

## V. SIMULATION RESULTS

### A. The Layer Model and the Zigzag-scan-based Permutation

We first check the layer model for the DCT2 coefficient matrix of the gray image: Boat ( $512 \times 512$ ). The format used in the simulation is tagged image file format (TIFF). The best  $s$ -term approximation is obtained by keeping all DCT2 coefficients with magnitudes not less than 1000 and changing the remaining to zeros. In Fig. 6, the x-axis is the layer index  $m$ , and y-axis is the probability of an element in the  $m$ -th layer of the best  $s$ -term approximation  $\mathbf{X}^s$  of the DCT2 coefficient matrix to be nonzero, calculated as  $p_m = (1/m) \sum_{i+j-1=m} \mathbf{I}(\mathbf{X}^s(i, j) \neq 0)$ , where  $\mathbf{I}(\cdot)$  is the indicator function. The  $p_m$ 's versus layer index  $m$  for the real image ‘‘Boat.tiff’’ and the result of the  $(r_0, r_1, r_2, \alpha)$ -layer model with  $r_0 = 0, r_1 = 3, r_2 = 32, \alpha = 0.15$  are shown in Fig. 6. It can be seen that the two curves are close to each other. Similar results are also achieved for other images. Then according to Proposition 1,

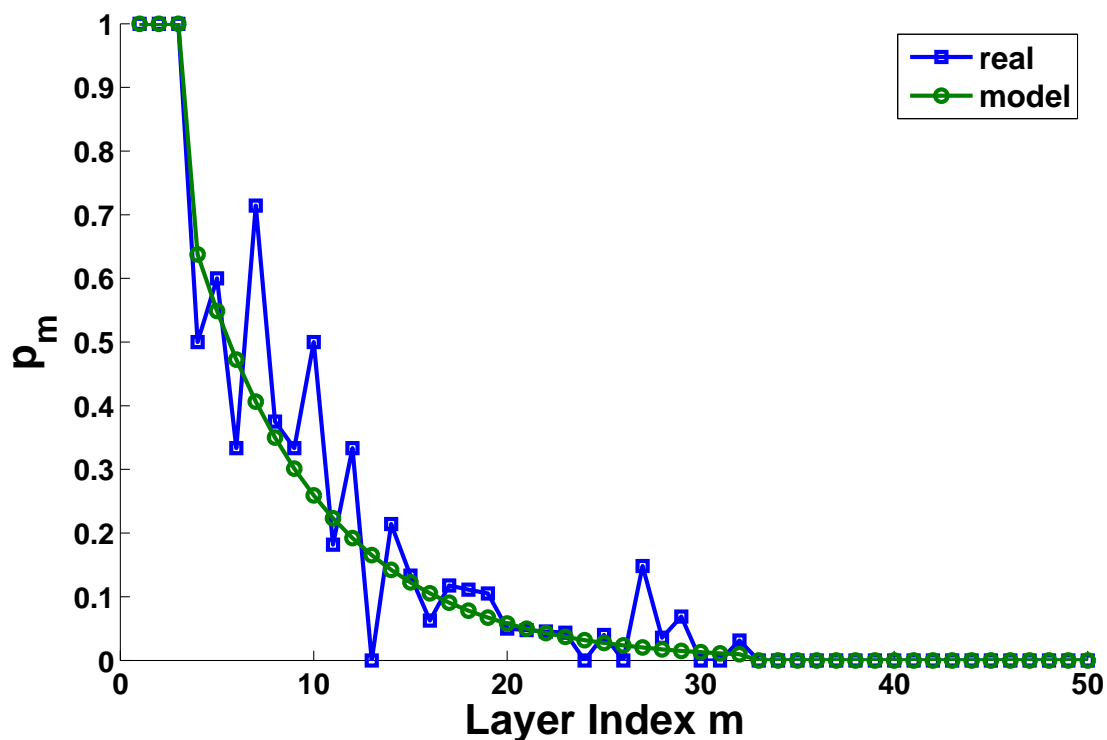


Fig. 6: Layer model of Boat.tiff.

TABLE I: Comparison of  $\|s\|_\infty$  before and after the zigzag-scan-based permutation.

Image	Magnitude Threshold			
	400	600	800	1000
Boat	33 vs. 2	23 vs. 2	19 vs. 2	16 vs. 1
Cameraman	13 vs. 2	8 vs. 2	7 vs. 1	4 vs. 1
Lena	14 vs. 3	11 vs. 2	8 vs. 1	7 vs. 1
Peppers	27 vs. 3	15 vs. 2	11 vs. 2	11 vs. 2

the zigzag-scan-based permutation is an acceptable permutation for DCT2 coefficient matrices of such images with an overwhelming probability.

The changes of  $\|s\|_\infty$  of the best  $s$ -term approximation of the DCT2 coefficient matrix before and after the zigzag-scan-based permutation are shown in Table I. The DCT2 coefficient matrices are taken from four test images: Boat ( $512 \times 512$ ), Lena ( $512 \times 512$ ), Cameraman ( $256 \times 256$ ), Peppers ( $512 \times 512$ ). The best  $s$ -term approximation is chosen according to different magnitude thresholds, i.e., keeping DCT2

coefficients whose magnitudes are not less than the magnitude threshold and setting the remaining to be zeros. Table I shows that  $\|s\|_\infty$  decreases significantly after the zigzag-scan-based permutation, which is consistent with Proposition 1.

### B. Image Compression via Parallel CS with the Zigzag-Scan-Based Permutation

The performance of image compression via parallel CS with the zigzag-scan-based permutation is shown by compressing the DCT2 coefficients of four images: Boat, Lena, Cameraman and Peppers. The PSNR is employed to show the reconstruction performance. We compare the performances of the parallel CS scheme for the configurations: 1) with no permutation; 2) with the zigzag-scan-based permutation. Entries of the sensing matrix  $\mathbf{A} \in \mathbb{R}^{K \times M}$  are drawn from Gaussian ensembles, with variance being  $1/K$ . The parallel CS reconstruction is implemented using basis pursuit algorithm by the CVX optimization toolbox.<sup>9</sup> Other reconstruction algorithms than the basis pursuit can also be used. PSNR performance for different methods is shown in Fig. 7 versus the compression ratio, which is the ratio of the number of measurements to the total number of elements in the DCT2 coefficient matrix.

From Fig. 7, we can see that under the same compression ratio, the zigzag-scan-based permutation helps to improve the PSNR by around 4 dB for all images. Consequently, it shows that the PSNR performance is indeed improved significantly after permutation.

### C. Video Compression via Parallel CS with the Zigzag-scan-based Permutation

The test video sequences in this example are three standard YUV video sequences: Akiyo, Foreman, Coastguard. The format used in the simulation is quarter common intermediate format (QCIF). The performance of the proposed video compression scheme is shown by compressing the luminance components of the first 10 frames, i.e., 5 reference frames and 5 non-reference frames. The average PSNR for reference frames and non-reference frames is used as performance metric. All settings are the same as in the example in Subsection V-B. PSNR performance for different methods is shown in Figs. 8 and 9 versus the average compression ratio, that is,  $(\text{compression ratio of reference frames} + \text{compression ratio of non-reference frames})/2$ .

From Fig. 8, we can see that under the same average compression ratio, the zigzag-scan-based permutation helps to improve the PSNR of reference frames by around 3~9 dB for Akiyo, 5~6 dB for Foreman and 4~8 dB for Coastguard. Fig. 9 shows that the zigzag-scan-based permutation also improves the PSNR

<sup>9</sup>The toolbox was downloaded at <http://cvxr.com/cvx>.

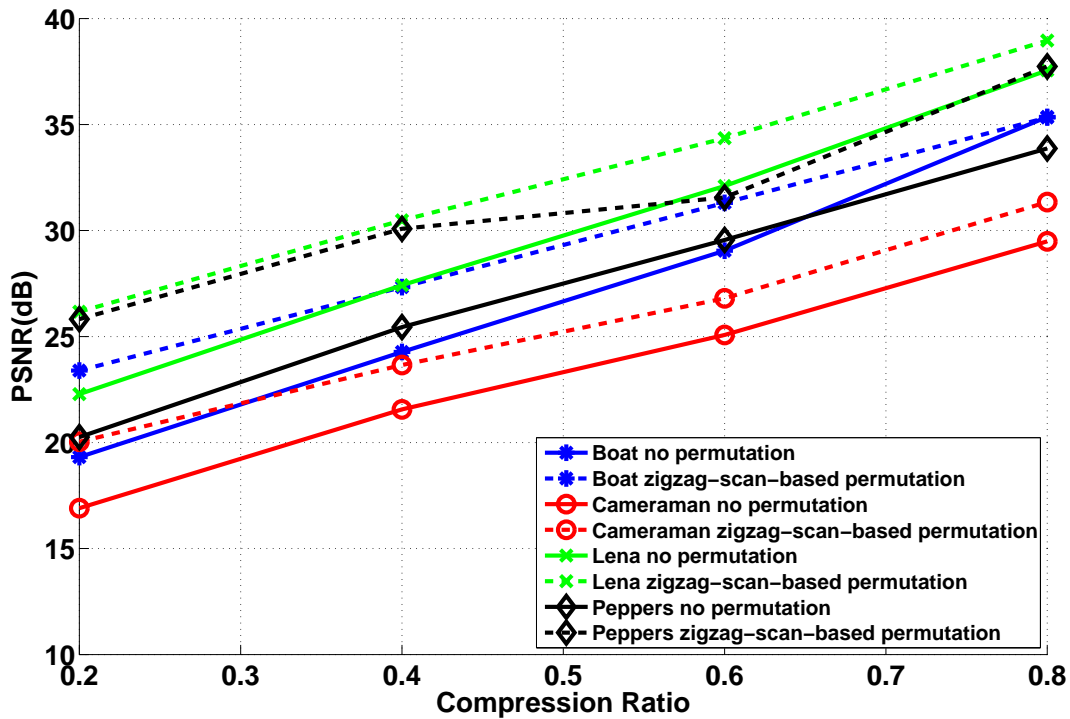


Fig. 7: PSNR for the parallel CS scheme with/without the zigzag-scan-based permutation in image compression.

performance of non-reference frames by around 3~9 dB for Akiyo, 2~5 dB for Foreman and 3~7 dB for Coastguard. The improved PSNR for the non-reference frame is a bit lower than that of the preceding reference frame because the reconstruction of the non-reference frame relies on both the reconstruction of its preceding reference frame and the reconstruction of difference between the non-reference frame and its preceding reference frame.

To show the advantage of the video compression scheme proposed in Section IV, we compare the total time of reconstructing one pair of reference and non-reference frames using (i) the video encoder and decoder employed in the C-DMRC system proposed in [27] and (ii) the video encoder and decoder proposed in Section IV. We also show the PSNRs of the reconstructed reference and non-reference frames for both schemes. The video sequence used in the simulation is the standard YUV sequence Akiyo (QCIF format). The measurement matrices used in the C-DMRC system and our scheme are the scrambled block Hadamard matrix (block length equals to 32) and the random Gaussian matrix,



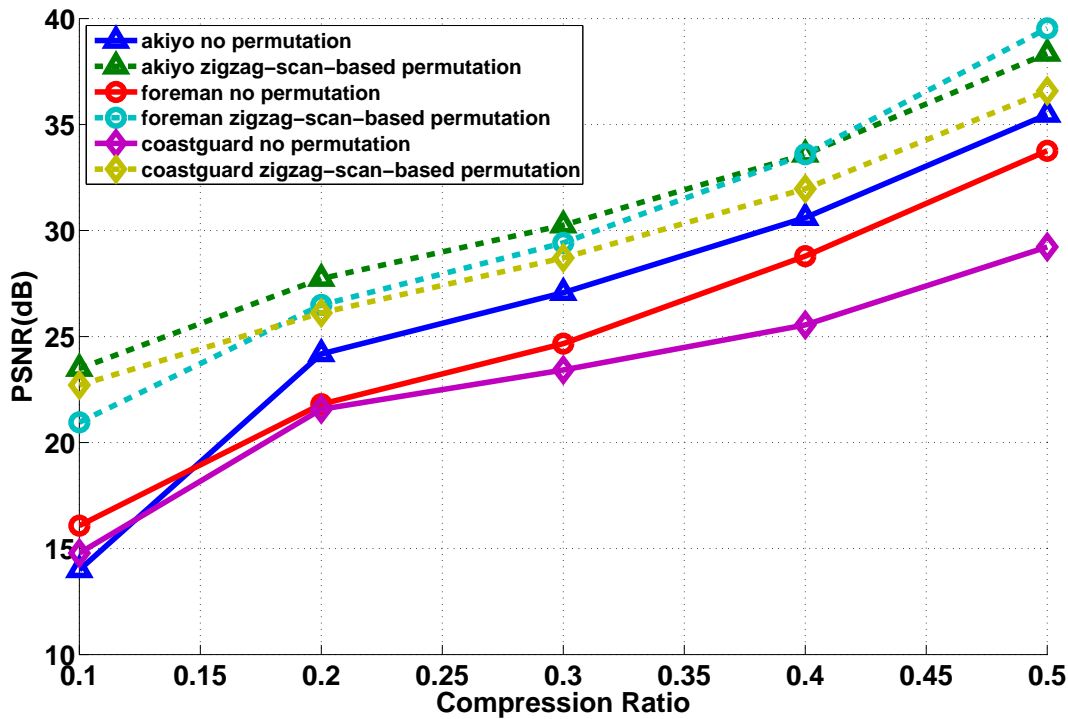


Fig. 8: Average PSNR of reconstructed reference frames.

respectively. The CS reconstruction algorithm is implemented using the  $l_1$ -magic package.<sup>10</sup> To eliminate the effects of randomness, we run 200 trials for each average compression ratio and show the average PSNR and total reconstruction time. The results are shown in Tables II and III.

It can be seen from Tables II and III that the reconstruction time using the video encoder and decoder proposed in Section IV is less than that for the video encoder and decoder employed in [27], especially when the compression ratio is low. In addition, if there are multiple decoding processors simultaneously reconstructing the columns of a video frame as shown in Fig. 5b, the reconstruction time can be further reduced approximately to the total reconstruction time divided by the number of decoding processors. It can also be observed in Table II that the time for reconstruction using the video encoder and decoder employed in [27] decreases as the average compression ratio increases. This is because the reconstruction algorithm converges faster as the number of measurements increases. According to Table III, the time for reconstruction using the video encoder and decoder proposed in Section IV is less sensitive to the

<sup>10</sup>The package is available at <http://users.ece.gatech.edu/~justin/l1magic>.

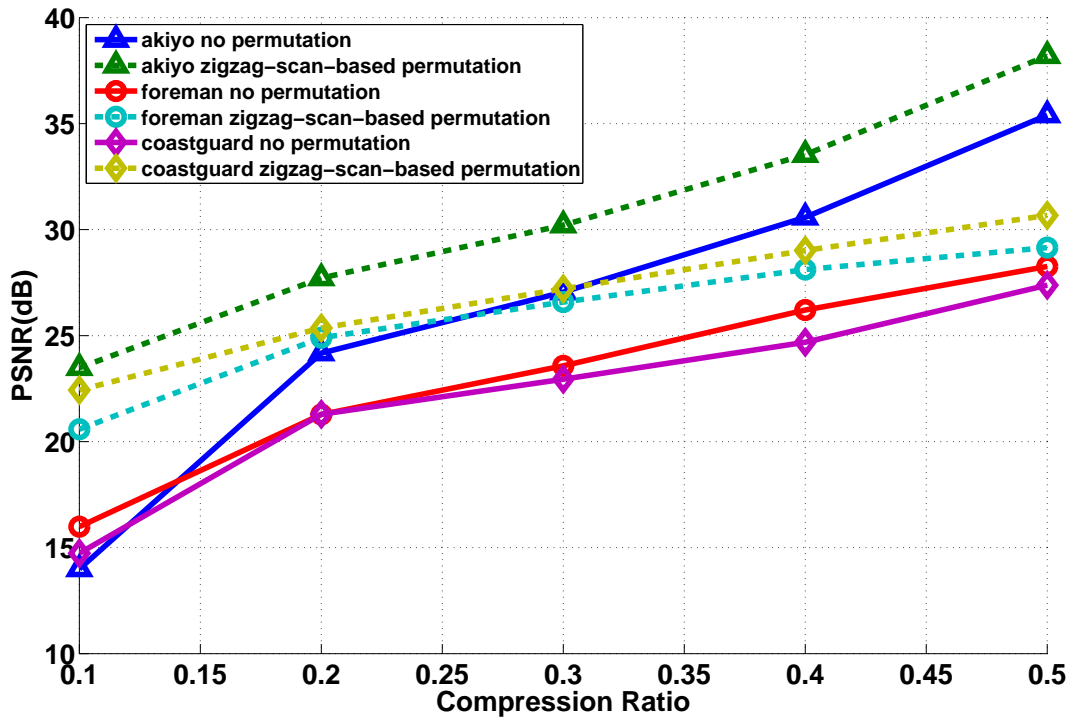


Fig. 9: Average PSNR of reconstructed non-reference frames.

TABLE II: Total reconstruction time and PSNR of reconstructed video frames using the video encoder and decoder employed in [27].

Average Compression Ratio		0.1	0.2	0.3	0.4	0.5
Reconstruction Time (seconds)		55.32	47.34	37.23	37.08	30.49
PSNR (dB)	Reference Frame	24.43	27.52	29.79	32.53	36.24
	Non-reference Frame	24.44	27.53	29.73	32.27	35.32

TABLE III: Total reconstruction time and PSNR of reconstructed video frames using the video encoder and decoder proposed in Section IV.

Average Compression Ratio		0.1	0.2	0.3	0.4	0.5
Reconstruction Time (seconds)		12.85	14.30	20.17	18.40	18.67
PSNR (dB)	Reference Frame	24.17	27.30	30.32	33.79	38.34
	Non-reference Frame	24.17	27.29	30.29	33.71	38.10

compression ratio. In addition, we can see that compared to the video encoder and decoder employed in [27], the PSNR of reconstructed video frames for the video encoder and decoder proposed in Section IV is larger when the average compression ratio is larger than 0.3, and is almost the same (less than 0.3dB degradation) when the average compression ratio is smaller than 0.3.

## VI. CONCLUSION AND DISCUSSION

A parallel CS scheme with permutation has been proposed. It has been proved that with a so-called acceptable permutation, the RIP condition for the sensing matrix in the parallel CS can be relaxed. The group-scan-based permutation has been introduced. As an example, the zigzag-scan-based permutation for 2D signals satisfying the  $(r_0, r_1, r_2, \alpha)$ -layer model, such as DCT2 coefficient matrices of 2D images, has been analyzed. The application to image and video compression has been discussed as well. In the simulations, it has been shown that the zigzag-scan-based permutation for DCT2 coefficient matrices of images is an acceptable permutation. In addition, the simulation results have shown that the proposed scheme improves the reconstruction performance of images and videos in terms of PSNR significantly.

Finally, it is worth mentioning that the zigzag-scan-based permutation is designed for signals satisfying the proposed layer model. If a signal has most of its large entries clustered around one or more fixed locations, the more general group-scan-based permutation is applicable. Similarly to the zigzag-scan-based permutation for the layer model, a lower bound on the probability that the group-scan-based permutation is an acceptable permutation can be derived given a mathematical model for the distribution pattern of large entries in the signal.

## VII. APPENDIX: PROOF OF PROPOSITION 1

*Proof:* Denote the  $j$ -th element of the sparsity vector  $\mathbf{s}$  as  $s_j$ , i.e., the sparsity level of the  $j$ -th column of  $\mathbf{X}^s$  is  $s_j$ . Since  $\mathbf{X}$  follows the  $(r_0, r_1, r_2, \alpha)$ -layer model, the nonzero elements in  $\mathbf{X}^s$  are all in layers of  $\mathbf{X}^s$  whose indices range from  $r_0 + 1$  to  $r_2$ . After performing the zigzag-scan-based permutation on  $\mathbf{X}^s$ , the maximal number of nonzero entries in any column is  $u = \lceil (r_0 + r_2 + 1)(r_2 - r_0) / 2N \rceil$ . Therefore,  $u \geq \|\mathbf{s}^\dagger\|_\infty$ . Let  $l = \lceil (r_0 + r_2 + 1) / 2 \rceil$ . Since  $r_2 \leq \min \{M, N\}$  and  $r_2 \geq 2r_1 - 3r_0 - 1$ , we have  $l \geq u$  and  $l \geq r_1 - r_0$ .

As a result, the probability that the zigzag-scan-based permutation of a 2D signal satisfying the  $(r_0, r_1, r_2, \alpha)$ -layer model is an acceptable permutation can be expressed as

$$\Pr \{ \mathbf{P} \text{ is acceptable} \} = \Pr \{ \|\mathbf{s}\|_\infty > \|\mathbf{s}^\dagger\|_\infty \} \quad (11a)$$

$$= \sum_{t=1}^{r_2-r_0} \Pr \{ \|\mathbf{s}\|_\infty = t, \|\mathbf{s}^\dagger\|_\infty \leq t-1 \} \quad (11b)$$

$$\geq \sum_{t=u+1}^{r_2-r_0} \Pr \{ \|\mathbf{s}\|_\infty = t, \|\mathbf{s}^\dagger\|_\infty \leq t-1 \} \\ = \sum_{t=u+1}^{r_2-r_0} \Pr \{ \|\mathbf{s}\|_\infty = t \} \quad (11c)$$

$$= \Pr \{ \|\mathbf{s}\|_\infty \geq u+1 \} = 1 - \Pr \{ \|\mathbf{s}\|_\infty \leq u \} \\ \geq 1 - \Pr \{ \|\mathbf{s}\|_\infty \leq l \}. \quad (11d)$$

To derive (11a), we have used the fact that an acceptable permutation must result in  $\|\mathbf{s}^\dagger\|_\infty < \|\mathbf{s}\|_\infty$ . For deriving (11b), we have used the fact that the maximal sparsity level among columns of the best  $s$ -term approximation  $\mathbf{X}^s$  is upper bounded by  $(r_2 - r_0)$ , i.e.,  $\|\mathbf{s}\|_\infty \leq r_2 - r_0$ , which immediately follows from the  $(r_0, r_1, r_2, \alpha)$ -layer model. For deriving (11c), we have used the fact that  $u \geq \|\mathbf{s}^\dagger\|_\infty$ . Finally, for deriving (11d), we have used the fact that  $u \leq l$ . Based on (11d), we focus on the cumulative distribution function of  $\|\mathbf{s}\|_\infty$ .

Since the events that  $s_j \leq l$  for different  $j$ 's are independent with each other, we have

$$\Pr \{ \|\mathbf{s}\|_\infty \leq l \} = \prod_{j=1}^N \Pr \{ s_j \leq l \}. \quad (12)$$

Moreover, since the position  $(i, j)$  of an element in  $\mathbf{X}^s$  indicates the index  $m$  of the layer where the

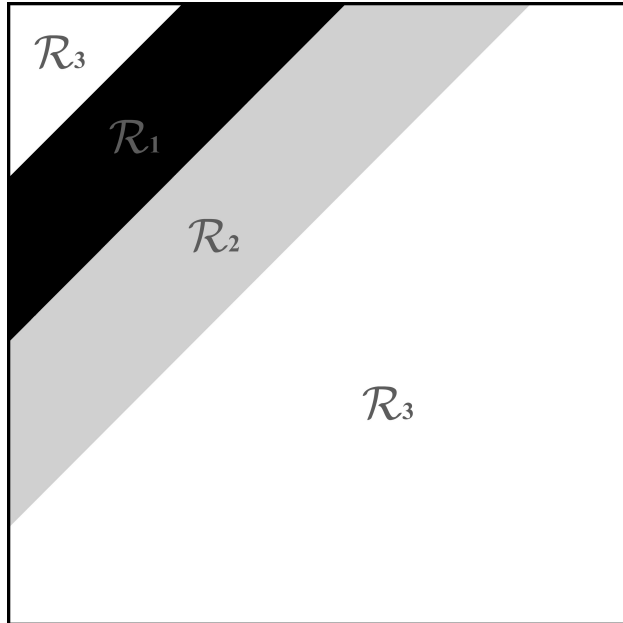


Fig. 10: Regions in the  $(r_0, r_1, r_2, \alpha)$ -layer model.

element is located, i.e.,  $m = i + j - 1$ , we can define three regions in  $\mathbf{X}^s$ :

$$\begin{aligned} \mathcal{R}_1 &= \{(i, j) \in \mathbb{Z}^2 | r_0 + 1 \leq i + j - 1 \leq r_1\} \\ \mathcal{R}_2 &= \{(i, j) \in \mathbb{Z}^2 | r_1 + 1 \leq i + j - 1 \leq r_2\} \\ \mathcal{R}_3 &= \{(i, j) \in \mathbb{Z}^2 | 1 \leq i + j - 1 \leq r_0\} \cup \\ &\quad \{(i, j) \in \mathbb{Z}^2 | r_2 + 1 \leq i + j - 1 \leq M + N - 1\}. \end{aligned}$$

These regions are separated by three transition layers, i.e., the  $r_0$ -th layer, the  $r_1$ -th layer and the  $r_2$ -th layer, and they are shown in Fig. 10. Therefore, according to Definition 5, all elements of  $\mathbf{X}^s$  are nonzero with probability 1 in region  $\mathcal{R}_1$ . In region  $\mathcal{R}_3$ , all elements of  $\mathbf{X}^s$  are zero with probability 1. In region  $\mathcal{R}_2$ , the probability of an element to be nonzero decreases exponentially with decay factor  $\alpha$  as the layer index  $m$  increases. We use  $p_m$  to denote the probability of an element in the  $m$ -th layer of  $\mathbf{X}^s$  to be nonzero.

For the  $j$ -th column of  $\mathbf{X}^s$ , if  $r_2 + 1 \leq j \leq N$ , all elements of the column are in region  $\mathcal{R}_3$  and thus are all zeros. We have  $\Pr\{s_j \leq l\} = 1$  since  $l \geq r_1 - r_0 \geq 1$ . According to (12), we have

$$\Pr\{\|\mathbf{s}\|_\infty \leq l\} = \prod_{j=1}^{r_2} \Pr\{s_j \leq l\} = \prod_{j=1}^{r_2} \sum_{k=0}^l \Pr\{s_j = k\}. \quad (13)$$

Consequently, we focus on the probability distribution of  $s_j$  for the first  $r_2$  columns of  $\mathbf{X}^s$ , i.e.,  $\Pr\{s_j = k\}$  for all  $0 \leq k \leq l$  and  $1 \leq j \leq r_2$ .

Let  $k_j$  denote the number of elements in the  $j$ -th column of  $\mathbf{X}^s$  that are in region  $\mathcal{R}_1$ , i.e.,

$$k_j = \begin{cases} r_1 - r_0, & 1 \leq j \leq r_0 \\ r_1 - j + 1, & r_0 + 1 \leq j \leq r_1 \\ 0, & r_1 + 1 \leq j \leq r_2. \end{cases}$$

Meanwhile, in the  $j$ -th column ( $1 \leq j \leq r_2$ ) of  $\mathbf{X}^s$ ,  $m_j = \max\{r_1 + 1, j\}$  and  $r_2$  are the starting and ending layer indices of region  $\mathcal{R}_2$ , respectively.

In (13), for  $1 \leq j \leq r_2$ , i.e., the first  $r_2$  columns of  $\mathbf{X}^s$ , we consider three cases depending on the value of  $k$ : 1)  $k = k_j$ ; 2)  $k_j + 1 \leq k \leq \min\{r_2 - r_0, r_2 - j + 1\}$ ; and 3)  $k \leq k_j - 1$  or  $k \geq \min\{r_2 - r_0 + 1, r_2 - j + 2\}$ .

For the first case, i.e.,  $k = k_j$ , it can be seen that the event that  $s_j = k$  happens when the elements of the  $j$ -th column of  $\mathbf{X}^s$  that are in the region  $\mathcal{R}_2$  are all zeros. Therefore, we have

$$\Pr\{s_j = k\} = \prod_{m=m_j}^{r_2} (1 - p_m). \quad (14)$$

For the second case, i.e.,  $k_j + 1 \leq k \leq \min\{r_2 - r_0, r_2 - j + 1\}$ , the event that  $s_j = k$  means that the  $j$ -th column of  $\mathbf{X}^s$  has  $(k - k_j)$  nonzero elements in the region  $\mathcal{R}_2$ . Denote indices of these  $(k - k_j)$  nonzero elements as  $a_1, a_2, \dots, a_{k-k_j}$  with  $a_1 < a_2 < \dots < a_{k-k_j}$ . So  $a_1, a_2, \dots, a_{k-k_j} \in \mathcal{A}_j \triangleq \{m_j, m_j + 1, \dots, r_2\}$ . We then have

$$\begin{aligned} & \Pr\{s_j = k\} \\ &= \sum_{\substack{a_1, a_2, \dots, a_{k-k_j} \in \mathcal{A}_j \\ a_1 < a_2 < \dots < a_{k-k_j}}} p_{a_1} \cdots p_{a_{k-k_j}} \prod_{\substack{m=m_j \\ m \neq a_i \\ i=1, \dots, k-k_j}}^{r_2} (1 - p_m) \\ &= \sum_{\substack{a_1, a_2, \dots, a_{k-k_j} \in \mathcal{A}_j \\ a_1 < a_2 < \dots < a_{k-k_j}}} \frac{p_{a_1} \cdots p_{a_{k-k_j}}}{(1 - p_{a_1}) \cdots (1 - p_{a_{k-k_j}})} \prod_{m=m_j}^{r_2} (1 - p_m) \\ &= \left[ \prod_{m=m_j}^{r_2} (1 - p_m) \right] \sum_{\substack{a_1, a_2, \dots, a_{k-k_j} \in \mathcal{A}_j \\ a_1 < a_2 < \dots < a_{k-k_j}}} \frac{p_{a_1} \cdots p_{a_{k-k_j}}}{(1 - p_{a_1}) \cdots (1 - p_{a_{k-k_j}})}. \end{aligned} \quad (15)$$

For the third case, i.e.,  $k \leq k_j - 1$  or  $k \geq \min\{r_2 - r_0 + 1, r_2 - j + 2\}$ , since  $k_j \leq s_j \leq \min\{r_2 - r_0, r_2 - j + 1\}$  for  $1 \leq j \leq r_2$ , the event that  $s_j = k$  never happens, i.e.,

$$\Pr\{s_j = k\} = 0. \quad (16)$$

According to (11d) and (13)-(16) and the fact that  $l \geq r_1 - r_0 \geq k_j$ , we have

$$\begin{aligned}
& \Pr \{P \text{ is acceptable}\} \\
& \geq 1 - \prod_{j=1}^{r_2} \left\{ \prod_{m=m_j}^{r_2} (1-p_m) + \sum_{k=k_j+1}^{\min\{l, r_2-r_0, r_2-j+1\}} \left[ \prod_{m=m_j}^{r_2} (1-p_m) \right] \sum_{\substack{a_1, a_2, \dots, a_{k-k_j} \in \mathcal{A}_j \\ a_1 < a_2 < \dots < a_{k-k_j}}} \frac{p_{a_1} \cdots p_{a_{k-k_j}}}{(1-p_{a_1}) \cdots (1-p_{a_{k-k_j}})} \right\} \\
& = 1 - \prod_{j=1}^{r_2} \left[ \prod_{m=m_j}^{r_2} (1-p_m) \right] \cdot \prod_{j=1}^{r_2} \left\{ 1 + \sum_{k=k_j+1}^{\min\{l, r_2-r_0, r_2-j+1\}} \sum_{\substack{a_1, a_2, \dots, a_{k-k_j} \in \mathcal{A}_j \\ a_1 < a_2 < \dots < a_{k-k_j}}} \frac{p_{a_1} \cdots p_{a_{k-k_j}}}{(1-p_{a_1}) \cdots (1-p_{a_{k-k_j}})} \right\} \\
& \stackrel{(a)}{=} 1 - \left[ \prod_{j=1}^{r_1} \prod_{m=r_1+1}^{r_2} (1-p_m) \cdot \prod_{j=r_1+1}^{r_2} \prod_{m=j}^{r_2} (1-p_m) \right] \cdot \prod_{j=1}^{r_2} \left\{ 1 + \sum_{k=k_j+1}^{\min\{l, r_2-r_0, r_2-j+1\}} \sum_{\substack{a_1, a_2, \dots, a_{k-k_j} \in \mathcal{A}_j \\ a_1 < a_2 < \dots < a_{k-k_j}}} \frac{p_{a_1} \cdots p_{a_{k-k_j}}}{(1-p_{a_1}) \cdots (1-p_{a_{k-k_j}})} \right\} \\
& = 1 - \left[ \prod_{m=r_1+1}^{r_2} (1-p_m)^{r_1} \cdot \prod_{m=r_1+1}^{r_2} (1-p_m)^{m-r_1} \right] \cdot \prod_{j=1}^{r_2} \left\{ 1 + \sum_{k=k_j+1}^{\min\{l, r_2-r_0, r_2-j+1\}} \sum_{\substack{a_1, a_2, \dots, a_{k-k_j} \in \mathcal{A}_j \\ a_1 < a_2 < \dots < a_{k-k_j}}} \frac{p_{a_1} \cdots p_{a_{k-k_j}}}{(1-p_{a_1}) \cdots (1-p_{a_{k-k_j}})} \right\} \\
& = 1 - \left[ \prod_{m=r_1+1}^{r_2} (1-p_m)^m \right] \cdot \prod_{j=1}^{r_2} \left\{ 1 + \sum_{k=k_j+1}^{\min\{l, r_2-r_0, r_2-j+1\}} \sum_{\substack{a_1, a_2, \dots, a_{k-k_j} \in \mathcal{A}_j \\ a_1 < a_2 < \dots < a_{k-k_j}}} \frac{p_{a_1} \cdots p_{a_{k-k_j}}}{(1-p_{a_1}) \cdots (1-p_{a_{k-k_j}})} \right\}.
\end{aligned}$$

where to obtain (a) we have used the fact that  $m_j = r_1 + 1$  for  $1 \leq j \leq r_1$  and  $m_j = j$  for  $r_1 + 1 \leq j \leq r_2$ . Using the facts that  $l = \lceil (r_0 + r_2 + 1)/2 \rceil$  and  $p_m = e^{-\alpha(m-r_0-1)}$  for  $r_1 + 1 \leq m \leq r_2$ , we obtain (10).

This completes the proof.  $\blacksquare$

## REFERENCES

- [1] D. L. Donoho, "Compressed sensing," *IEEE Trans. Inf. Theory*, vol. 52, no. 4, pp. 1289–1306, Apr. 2006.
- [2] E. J. Candès and T. Tao, "Near-optimal signal recovery from random projections: Universal encoding strategies?" *IEEE Trans. Inf. Theory*, vol. 52, no. 12, pp. 5406–5425, Dec. 2006.
- [3] —, "Decoding by linear programming," *IEEE Trans. Inf. Theory*, vol. 51, no. 12, pp. 4203–4214, Dec. 2005.
- [4] M. B. Wakin, J. N. Laska, M. F. Duarte, D. Baron, S. Sarvotham, D. Takhar, K. F. Kelly, and R. G. Baraniuk, "Compressive imaging for video representation and coding," in *Proc. Picture Coding Symp.*, Beijing, China, Apr. 24–26, 2006.
- [5] P. Nagesh and B. Li, "Compressive imaging of color images," in *Proc. IEEE Int. Conf. Acoustics, Speech and Signal Process.*, Taipei, Taiwan, Apr. 19–24, 2009, pp. 1261–1264.
- [6] M. F. Duarte and R. G. Baraniuk, "Kronecker compressive sensing," *IEEE Trans. Image Process.*, vol. 21, no. 2, pp. 494–504, Feb. 2012.
- [7] Y. Rivenson and A. Stern, "Compressed imaging with a separable sensing operator," *IEEE Signal Process. Lett.*, vol. 16, no. 6, pp. 449–452, Jun. 2009.
- [8] L. Gan, "Block compressed sensing of natural images," in *Proc. Int. Conf. Digital Signal Process.*, Cardiff, UK, Jul. 1–4, 2007, pp. 403–406.
- [9] S. Mun and J. Fowler, "Block compressed sensing of images using directional transforms," in *Proc. Int. Conf. Image Process.*, Cairo, Egypt, Nov. 7–10, 2009, pp. 3021–3024.
- [10] L. Gan, T. T. Do, and T. D. Tran, "Fast compressive imaging using scrambled block Hadamard ensemble," in *Proc. 16th European Signal Process. Conf.*, Lausanne, Switzerland, Aug. 25–29, 2008.
- [11] E. J. Candès, J. Romberg, and T. Tao, "Stable signal recovery from incomplete and inaccurate measurements," *Comm. Pure Appl. Math.*, vol. 59, no. 8, pp. 1207–1223, Aug. 2006.
- [12] E. J. Candès and J. K. Romberg, "Signal recovery from random projections," in *Proc. SPIE-IS&T Electronic Imaging*, San Jose, CA, USA, Jan. 17–18, 2005, pp. 76–86.
- [13] B. Han, F. Wu, and D. Wu, "Image representation by compressed sensing," in *Proc. 15th IEEE Int. Conf. Image Process.*, San Diego, California, USA, Oct. 12–15, 2008, pp. 1344–1347.



- [14] J. Wu, F. Liu, L. C. Jiao, X. Wang, and B. Hou, "Multivariate compressive sensing for image reconstruction in the wavelet domain: using scale mixture models," *IEEE Trans. Image Process.*, vol. 20, no. 12, pp. 3483–3494, Dec. 2011.
- [15] Y. Kim, M. S. Nadar, and A. Bilgin, "Wavelet-based compressed sensing using a Gaussian scale mixture model," *IEEE Trans. Image Process.*, vol. 21, no. 6, pp. 3102–3108, Jun. 2012.
- [16] V. Stanković, L. Stanković, and S. Cheng, "Compressive sampling of binary images," in *Proc. Cong. on Image and Signal Process.*, Sanya, Hainan, China, May 27–30, 2008, pp. 7–11.
- [17] —, "Compressive video sampling," in *Proc. 16th European Signal Process. Conf.*, Lausanne, Switzerland, Aug. 25–29, 2008, pp. 2–6.
- [18] Z. Liu, A. Y. Elezzabi, and H. V. Zhao, "Maximum frame rate video acquisition using adaptive compressed sensing," *IEEE Trans. Circuits Syst. Video Technol.*, vol. 21, no. 11, pp. 1704–1718, Nov. 2011.
- [19] S. F. Cotter, B. D. Rao, K. Engan, and K. Kreutz-Delgado, "Sparse solutions to linear inverse problems with multiple measurement vectors," *IEEE Trans. Signal Process.*, vol. 53, no. 7, pp. 2477–2488, Jul. 2005.
- [20] J. Chen and X. Huo, "Theoretical results on sparse representations of multiple-measurement vectors," *IEEE Trans. Signal Process.*, vol. 54, no. 12, pp. 4634–4643, Dec. 2006.
- [21] E. van den Berg and M. P. Friedlander, "Theoretical and empirical results for recovery from multiple measurements," *IEEE Trans. Inf. Theory*, vol. 56, no. 5, pp. 2516–2527, May 2010.
- [22] O. Taheri and S. A. Vorobyov, "Segmented compressed sampling for analog-to-information conversion: Method and performance analysis," *IEEE Trans. Signal Process.*, vol. 59, no. 2, pp. 554–572, 2011.
- [23] M. F. Duarte, S. Jafarpour, and A. R. Calderbank, "Performance of the Delsarte-Goethals frame on clustered sparse vectors," *IEEE Trans. Signal Process.*, vol. 61, no. 8, pp. 1998–2008, Apr. 2013.
- [24] H. Fang, S. A. Vorobyov, H. Jiang, and O. Taheri, "2D signal compression via parallel compressed sensing with permutations," in *Proc. 46th Annual Asilomar Conf. Signals, Systems, and Computers*, Pacific Grove, California, USA, Nov. 4–7, 2012, pp. 1925–1929.
- [25] E. J. Candès and M. B. Wakin, "An introduction to compressive sampling," *IEEE Signal Process. Mag.*, vol. 25, no. 2, pp. 21–30, Mar. 2008.
- [26] G. K. Wallace, "The JPEG still picture compression standard," *IEEE Trans. Consum. Electron.*, vol. 38, no. 1, pp. 18–34, Feb. 1992.
- [27] S. Pudlewski, T. Melodia, and A. Prasanna, "Compressed-sensing-enabled video streaming for wireless multimedia sensor networks," *IEEE Trans. Mobile Comput.*, vol. 11, no. 6, pp. 1060–1072, Jun. 2012.